Unclassified

(2)

AD-A250 767

REPORT DOCUMENTATION PAGE

DTIC ELECTE MAY 14 1992 S D

1b RESTRICTIVE MARKINGS

3 DISTRIBUTION/AVAILABILITY OF REPORT
Approved for public release; distribution unlimited.

2b DECLASSIFICATION/DOWNGRADING SCHEDULE

4 PERFORMING ORGANIZATION REPORT NUMBER(S)

5 MONITORING ORGANIZATION REPORT NUMBER(S)
AFOSR-TR- 92 0313

6a NAME OF PERFORMING ORGANIZATION
Joint Institute for Laboratory Astrophysics

6b. OFFICE SYMBOL (If applicable)

7a. NAME OF MONITORING ORGANIZATION
Air Force Office of Scientific Research

6c. ADDRESS (City, State and ZIP Code)
University of Colorado
Campus Box 440
Boulder, CO 80309-0440

7b. ADDRESS (City, State and ZIP Code)
Department of the Air Force
Bolling Air Force Base, DC 20332-6448

8a NAME OF FUNDING/SPONSORING ORGANIZATION
Air Force Office of Scientific Research

8b. OFFICE SYMBOL (If applicable)
NE

9 PROCUREMENT INSTRUMENT IDENTIFICATION NUMBER
AFOSR-90-0198

8c ADDRESS (City, State and ZIP Code)
Department of the Air Force
Bolling Air Force Base, DC 20332-6448

10. SOURCE OF FUNDING NOS.

PROGRAM ELEMENT NO.	PROJECT NO.	TASK NO.	WORK UNIT NO
61102F	2301 A5	A1	

11 TITLE (Include Security Classification) Applications of the photorefractive effect and damage induced effects in fibers

12. PERSONAL AUTHOR(S)
Dana Z. Anderson

13a. TYPE OF REPORT	13b. TIME COVERED	14. DATE OF REPORT (Yr., Mo., Day)	15. PAGE COUNT
Annual	FROM 11/1/90 TO 10/31/91	March 26, 1992	

16 SUPPLEMENTARY NOTATION

17. COSATI CODES			18. SUBJECT TERMS (Continue on reverse if necessary and identify by block number)
FIELD	GROUP	SUB. GR.	Nonlinear optics, photorefractive effects

19. One aspect of this work concerns the processes of self-organized second-harmonic generation in fibers. We have experimentally investigated the nature of grating formation in the glass fibers and found it to be reversible. That is, a grating can be repetitively written, erased, and re-written. We have also shown that the grating erasure follows a power-law time dependence and explain the dependence as a consequence of the transverse mode structure of the fields in the fiber. Numerical work has focused on the microscopic aspect of ionization from a model defect potential. We have integrated Schrödinger's equation exactly in the one-dimensional case. Results so far indicate that a photovoltaic explanation of second-harmonic generation in fibers is robust against variation of the physical parameters of the model. The second aspect concerns the dynamics and self-organization of photorefractive optical circuits. We have produced circuits that self-organize according to the nature of their time dependent input. After self-organizing they process information in an adaptive and useful way. Our most highly developed circuit is a demultiplexer that separates signals from a multimode fiber.

20 DISTRIBUTION/AVAILABILITY OF ABSTRACT
UNCLASSIFIED/UNLIMITED ☐ SAME AS RPT. ☐ OTIC USERS ☐

21. ABSTRACT SECURITY CLASSIFICATION
Unclassified

22a. NAME OF RESPONSIBLE INDIVIDUAL	22b TELEPHONE NUMBER (Include Area Code)	22c. OFFICE SYMBOL
Schlossberg	(202) 767-4906	NE

DD FORM 1473, 83 APR EDITION OF 1 JAN 73 IS OBSOLETE.

SECURITY CLASSIFICATION OF THIS PAGE

A Report on AFOSR Contract #AFOSR 90-0198

APPLICATIONS OF THE PHOTOREFRACTIVE EFFECT AND DAMAGE INDUCED EFFECTS IN FIBERS

Submitted to

THE AIR FORCE OFFICE OF SCIENTIFIC RESEARCH

by

Dana Z. Anderson
Department of Physics and Joint Institute for Laboratory Astrophysics
University of Colorado, Boulder, CO 80309-0440

APPLICATIONS OF THE PHOTOREFRACTIVE EFFECT AND DAMAGE INDUCED EFFECTS IN FIBERS

INTRODUCTION

This is a report of work carried out under AFOSR contract #AFOSR 90-0198. The focus is two-fold. One aspect concerns the processes of self-organized second-harmonic generation in fibers. We have experimentally investigated the nature of grating formation in the glass fibers and found it to be reversible. That is, a grating can be repetitively written, erased, and re-written. We have also shown that the grating erasure follows a power-law time dependence and explain the dependence as a consequence of the transverse mode structure of the fields in the fiber. Numerical work has focused on the microscopic aspect of ionization from a model defect potential. We have integrated Schrödinger's equation exactly in the one-dimensional case. Results so far indicate that a photovoltaic explanation of second-harmonic generation in fibers is robust against variation of the physical parameters of the model.

The second aspect concerns the dynamics and self-organization of photorefractive optical circuits. We have produced circuits that self-organize according to the nature of their time dependent input. After self-organizing they process information in an adaptive and useful way. Our most highly developed circuit is a demultiplexer that separates signals from a multimode fiber.

The remainder of the report gives a more detailed account of the work, beginning in section 1 with a description of the experimental work on second-harmonic generation in fibers. Section 2 discusses some of the numerical work that has provided useful insight into the microscopic nature of the problem. Section 3 covers the work on self-organizing photorefractive circuits.

1. SECOND-HARMONIC GENERATION IN FIBERS

The phenomena of second-harmonic generation in fibers[1] is interesting from both fundamental and practical point of view. Conversion of a fundamental to its second-harmonic is not supposed to be possible in glass fibers, yet it can happen very efficiently after some preparation of the fiber. In some circumstances the fiber appears to prepare itself, and in this sense the phenomena is apparently self-organizing. Understanding this self-organization process is a challenge from a fundamental physics point of view. From a practical standpoint, if this phenomena can be controlled and be made very efficient, it is a potentially very low cost means of second-harmonic generation.

Recently the principal investigator and collaborators proposed a model for the self-organized process.[2] Herein we shall refer to this work as AMS-91. The model process consists of three steps: 1)The ionization of defect sites occurs in such a way that there is a *phase dependent* preferred direction for photoelectron emission. This preference arises from interference between various multiphoton ionization pathways to ionization. 2)Charge redistribution. Once freed from their traps, the charges redistribute, causing a local space charge field whose direction depends locally on the relative phase between the fundamental wave and its second harmonic. This dc electric field breaks the centrosymmetry of the fiber and permits, locally, second-harmonic generation. Space

charge field brings about an effective $\chi^{(2)}$ through the third-order nonlinear susceptibility of the glass. Because the effective $\chi^{(2)}$ varies spatially at the phase-mismatch frequency between the fundamental and its second harmonic, it is referred to as a $\chi^{(2)}$ grating. 3)Evolution of the second-harmonic field as governed by the slowly varying envelope equation derived through Maxwell's equations. In order for there to be *growth* of the second-harmonic light, there must be self-consistency between the second harmonic light generated by the presence of the space charge field and the second-harmonic light that was responsible for the space-charge field in the first place.

In this past year we have experimentally investigated a number of aspects of the dynamics associated with second-harmonic generation. First, we have found that the process of writing a $\chi^{(2)}$ grating is reversible: the grating can be erased by exposure purely to the second-harmonic and rewritten by simultaneous exposure to the fundamental and its second-harmonic. Second, we have found that the grating erases with a power law dependence. While one might expect an exponential decay law, one can show that the power law can arise simply by considering the transverse structure of the fields as determined by the modes of the fiber. However, we also found, unexpectedly, that the power law is itself dependent on the erasure intensity.

We have also performed some numerical calculations that integrate Schrödinger's equation exactly for a one-dimensional model potential. This has given us a chance to compare our perturbation theory calculation with a more exact numerical study. Qualitatively the analytical and numerical approaches are similar, yet the numerical version is showing some aspects that the simpler analytical version does not reveal. Of particular importance is that the phase between the $\chi^{(2)}$ grating and the multiphoton interference process which created it is dependent on the intensities of the fundamental and second-harmonic.

Reversibility

In understanding the charge transport phenomena it is crucial to know whether or not the grating formation process is reversible or not. The question is, do charges become repeatedly ionized and re-trapped, or does some species of trap change in some permanent way? The dynamics of the process will be drastically different in the two cases. If the process is similar to most photorefractive effects, then it is reversible. On the other hand, the related process of Hill grating formation in fibers appears not to be reversible. We performed a series of grating writing with subsequent incoherent erasure experiments on a single, short length of fiber. After erasure the $\chi^{(2)}$ grating was rewritten. We found that we could cycle many times from no grating to saturation to the same maximum level, indicated that the process of grating formation is indeed reversible. In addition to the knowledge that the grating is reversible, this finding has simplified the experimental work since we can be confident that we can do a series of experiments on a single fiber with the worry of trap depletion. In the past, each experiment employed a virgin fiber.

Figure 1.1 shows the experimental apparatus for the erasure experiments. Figure 1.2 shows the experimental results from a reversibility experiment. The curves show the amount of second-harmonic generated by the $\chi^{(2)}$ grating. The grating is written by exposing the fiber to the fundamental and its second-harmonic simultaneously. The data is obtained by blocking the imposed second-harmonic and measuring the amount generated by the fiber. In this case the fiber was exposed to the fundamental and its second-harmonic until the generated light reached saturation. The grating was subsequently erased by exposing the fiber to the second-harmonic light alone. At intervals, the grating strength was measured by blocking the second-harmonic and illuminating the fiber once again with the fundamental wave briefly. Here we have cycled through the writing erasure process several times. There is no sign of "fatigue" of any kind, indicating the processes is indeed reversible.

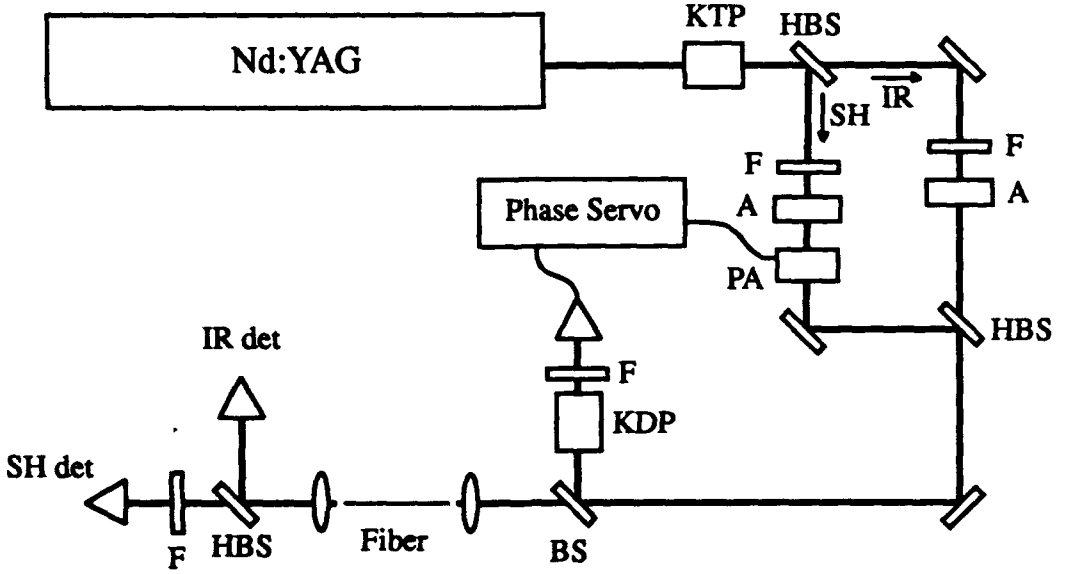

Figure 1.1. Experimental apparatus for reversibility, erasure and grating enhancement experiments. Filters F block unwanted wavelength (second-harmonic or fundamental). A seed second-harmonic beam is generated with a KTP crystal and separated from its fundamental with a harmonic beamsplitter HBS. Intensities are adjusted with attenuators A. The relative phase between the fundamental and second-harmonic is measured using an auxiliary second-harmonic generating crystal KDP and maintained using a phase-locked loop servo controlling a phase adjuster PA.

Erasure dynamics

From our model of second-harmonic generation in fibers we expect the processes to be mediated either by two photons or by four photons of the fundamental frequency and correspondingly by one or two photons of its second harmonic. So that we could

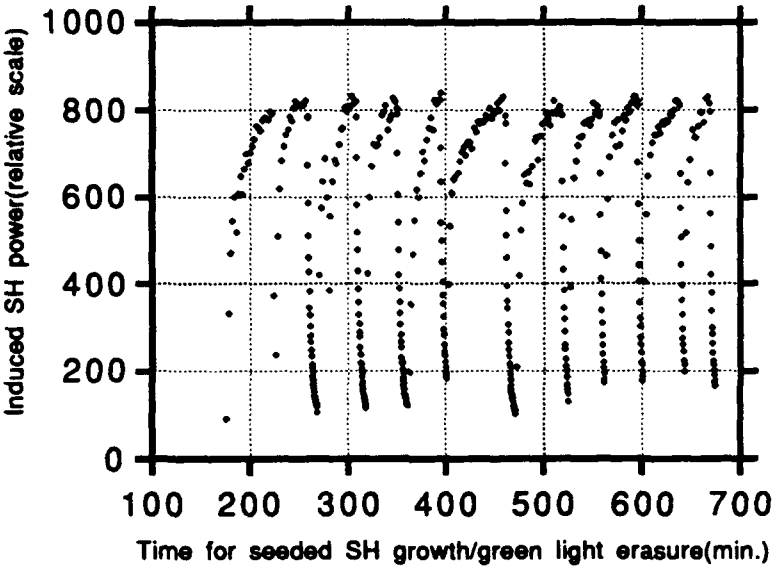

Figure 1.2. Repetitive growth and erasure of generated second-harmonic light. Points indicate generated second-harmonic intensity. In each cycle, a $\chi^{(2)}$ grating is written to saturation of the generated second-harmonic by illuminating the fiber with both the second-harmonic and its fundamental. After the generated light saturates, the grating is erased by illuminating the fiber with second-harmonic light only.

determine the number of fundamental photons involved we performed a series of $\chi^{(2)}$ grating erasure experiments. Here a grating is written using both infrared and its second harmonic, and then erasing the grating with the second-harmonic light only. The power dependence of the erasure rate should indicate the number of photons responsible for ionizing trapped charges.

As also observed by other researchers, we saw a power law dependence of the grating strength. Figure (3) shows a typical erasure curve fit to a power law decay. The grating strength is inferred by the intensity of the generated second-harmonic. We expect that the second-harmonic intensity is proportional to the square of the grating amplitude. Our explanation for the power law dependence is, however, different than that of other researchers. We show here that the power law dependence can arise simply from the transverse structure of the fiber modes. We start by assuming that the decay of the grating is fundamentally exponential in nature, but that the decay coefficient depends upon the intensity of the erasing beam to some power:

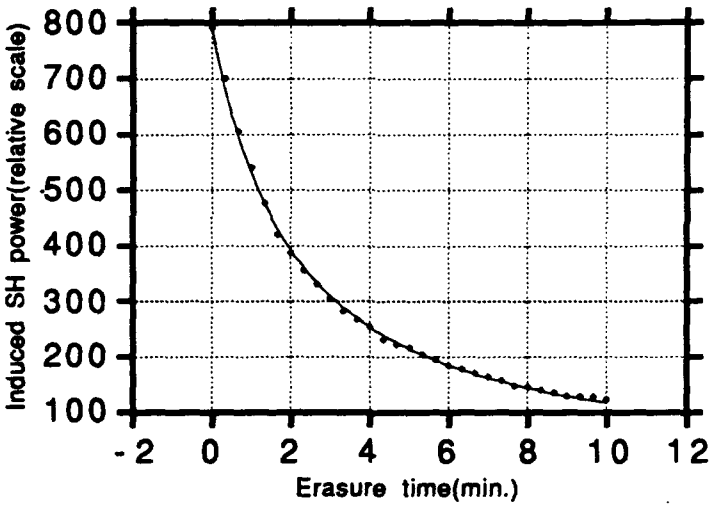

Figure 3. Decay of generated second-harmonic as $\chi^{(2)}$ grating is erased. The points are experimental data, the curve is fitted to a power law dependence (solid curve).

$$\dot{G} = \alpha_0 I^{\beta} G \tag{1.1}$$

Here α_0 is the decay rate proportionality constant and I is understood to be the erasure intensity. Now all the optical fields have a strong transverse intensity profile, which, for the sake of being specific we will assume to be Gaussian:

$$I(r) = \frac{I_0}{\pi r_0^2} \exp\left\{-(r/r_0)^2\right\}, \tag{1.2}$$

with r being the transverse radial coordinate and r_0 the beam radius. Thus, first, the grating decays at different rates at different transverse locations and, second, the contribution to the generated second-harmonic intensity is also dependent on transverse location. Integrating Eqn. (1.1) locally and using r to indicate the transverse radial component:

$$G(r,t) = G(r,0) \exp\left\{-t\alpha_0 \left(\frac{I_0}{\pi r_0^2}\right)^{\beta} e^{-\beta(r/r_0)^2}\right\}. \tag{1.3}$$

The second-harmonic field strength is given by an overlap integral involving the grating amplitude, the square of the fundamental field strength, and the transverse mode profile

of the second harmonic. We assume that the fundamental mode (intensity) beam radius is half that of the second-harmonic. In that case:

$$E_{2\omega}(t) \propto 2\pi \int_0^{\infty} \left[G(r,0) \exp\left\{ -t\alpha_0 \left(\frac{I_0}{\pi r_0^2} \right)^{\beta} e^{-\beta (r/r_0)^2} \right\} \right] \times \left[\frac{I_\omega}{\pi r_0^2} \exp\left\{ -\left(r/\sqrt{2} r_0 \right)^2 \right\} \right] \left[\frac{1}{\pi r_0^2} \exp\left\{ -\left(r/\sqrt{2} r_0 \right)^2 \right\} \right] r dr \tag{1.4}$$

The first bracketed factor is the grating strength, the next bracketed factor is the square of the fundamental field strength and the last factor is the second-harmonic mode profile. This ungainly expression can be simplified by making the transformations:

$$u \equiv \exp\left\{ -\beta \left(r / r_0 \right)^2 \right\}, \tag{1.5a}$$

$$\tau \equiv t\alpha_0 \left(\frac{I_0}{\pi r_0^2} \right)^{\beta}, \tag{1.5b}$$

whence:

$$E_{2\omega}(\tau) \propto \frac{I_\omega}{\beta \pi r_0^2} \int_0^1 G(u,0) u^{\left(\frac{1}{\beta} - 1 \right)} e^{-u\tau} du. \tag{1.6}$$

To integrate Eqn. (1.6) we need to know the initial grating amplitude, $G(u,0)$. Almost whatever the form for the initial grating, Eqn. (1.6) will give a power law at least for long times. For example, if we assume that the initial grating is everywhere constant and that the erasure rate is proportional to the incident intensity, ($\beta = 1$) then $E_{2\omega}(\tau) \propto 1/\tau$ and therefore the second-harmonic intensity falls inversely proportional to t^2. As β increases, so the power of t with which the second-harmonic decays *decreases* (i.e. $I_{2\omega} \propto t^{-2/\beta}$.

Our experimental results suggest β is of order unity (see below). One problem in drawing our conclusions too far is that we do not know the initial grating distribution particularly well, and our assumption that the fundamental has twice the beam intensity radius of the second-harmonic is not exact.

We see from Eqn. (1.5b) that the dimensionless time $\tau \propto I_0^{\beta}$. In other words, the decay coefficient of the grating should be proportional to the β^{th} power of the erasure power.

Our initial intention in the erasure experiments was to determine β by varying the erasure intensity. In this way we could determine the number of photons involved in the erasure process. We expected, as indicated, that the erasure process would involve either 1 or 2 photons of the second-harmonic light. To our surprise, however, we find that β is itself dependent upon the erasure intensity. Roughly, as the power varies over a factor of three, so does β, but inversely. Our current analysis shows that β varies from about 0.9 to 2.6. A better estimate taking into account the actual beam profiles is currently under way. The interpretation of these results says that the number of photons involved varies between 0.9 and 2.6 with an erasure power dependence. One explanation for this dependence suggests that an intermediate level may play a role and that ionization is a two-step process. The 2.6 power indicates that at low intensities three photons may be involved. One scenario is that a metastable level is excited by a two-photon transition, and then it is ionized by one more photon. This would be consistent with the known transition at 240nm and metastable state decaying with a 400nm fluorescence. If two steps are involved, then the power dependence of the erasure rate should vary from three photons at very low erasure powers to 1 photon at high powers as the population of the intermediate level becomes saturated. Unfortunately, we are limited on the high power end by fiber damage and on the low power end by exceedingly slow erasure rates, on the order of many hours. Thus we cannot in practice necessarily see the full power dependence of the erasure rate to prove definitively the existence of an intermediate level. Evidence of an intermediate level has also been found by Margulis in a very different set of experiments.

A publication reporting the above findings is now in preparation. Current work involves a more careful numerical analysis of the data, taking into account the actual mode profiles, core sizes and reasonable estimations for the initial grating amplitude transverse distribution.

Grating enhancement experiments

In the conventional photorefractive effect, the two-beam coupling gain of a drift-dominated medium can be enhanced by imposing a small frequency difference between the two beams. The reason for this is simple. In a drift-dominated medium the interference pattern caused by two, frequency degenerate beams is stationary and 90° out of phase with the induced index of refraction grating. No energy coupling can take place with this value of phase shift. By frequency shifting one beam relative to the other, the interference pattern moves and so does the induced grating. However, because of the finite time response of the medium, the grating lags behind the interference pattern. Thus, there is no longer a 90° phase difference between the two and energy coupling can take place. Measurements of the phase of the $\chi^{(2)}$ grating relative to the interference between twice the fundamental and the second-harmonic reveals approximately 90°. We expected that the efficiency of second-harmonic generation therefore to increase by putting a slight frequency shift on the seen second-harmonic. The frequency shift in our experiments was achieved by locking to an intensity maximum of the generated second-harmonic light --the locking was done with a phase-lock loop feeding back to a piezo mirror controlling the phase of the seed beam. The feedback scheme should force the phase between the seed and the fundamental to have the optimum phase for conversion of the second-harmonic. To our surprise, the phase locking experiment revealed *decreased* production of second-harmonic light.

2. MODEL NUMERICAL CALCULATIONS

The model in AMS-91 was based on a time-independent perturbation calculation in which the ionized electron states were taken to be free particle plane waves. In other words, it does not take into account scattering of the ionized electrons from the trapping potential. Furthermore, most experimental investigations have used pulsed lasers (e.g., mode-locked and Q-switched Nd:YAG) with powers approaching the damage threshold of the glass. Consequently, it is unclear whether a perturbative approach is applicable. While an analytic calculation as in AMS-91 provides insight into the basic physics, it is not clear to what extent the qualitative conclusions remain as the simplifying assumptions are eradicated.

In collaboration with L. You, J. Mostowski and J. Cooper, we have begun a numerical study of the interference induced asymmetric photoemission of electrons from a one-dimensional model potential. We perform a time-dependent numerical integration of Schrödinger's equation beginning with an electron in the ground-state of the potential. Scattering of the ionized electrons from the potential is implicitly taken into account by the calculation.

The single electron at the trap site is modeled as an electron bound to a one-dimensional short-range attractive potential:

$$V(\vec{x}) = -V_0 / \cosh^2(x/a), \tag{2.1}$$

with a range of the order of the parameter a.

This one-dimensional potential has analytical eigenvalue and eigenvector solutions for the bound and excited states. The interaction with the external electric field is taken to be $e\vec{p}\cdot\vec{A}(t)/mc + e^2A^2(t)/2mc^2$, which comes from the minimum coupling form of the Hamiltonian (the quadratic term can be neglected since under the dipole approximation it will only introduce a constant phase), and where $\vec{E}(t) = -\partial\vec{A}/\partial(ct)$. Here e denotes the electron charge, c the speed of the light, $\vec{p}$ the electron canonical momentum, and $\vec{E}$ the external laser field. The Schrödinger equation describing the model atom subject to the strong laser field is:

$$i\hbar\frac{\partial}{\partial t}\Psi(x,t) = [\frac{\vec{P}^2}{2m} + V(x)]\Psi(x,t), \tag{2.2}$$

where $\vec{P} = \vec{p} - e\vec{A}/c$ is the kinetic momentum, and where the initial condition is specified by some $\Psi(\vec{r},0)$. As we only consider the local ionization process at a given z, the external electromagnetic field is taken to be of the following form

$$\vec{E}(t) = \vec{e}_x E_\omega(t)\sin(\omega t) + \vec{e}_x E_{2\omega}(t)\sin[2\omega t + \phi(z)]. \tag{2.3}$$

The envelope functions determining the amplitudes of the fields are

$$E_{\omega_j}(t)=\begin{cases}E_{\omega_j 0}\sin^2(\pi t/2\tau), & 0<t<\tau;\\ E_{\omega_j 0} & \tau<t,T+\tau;\\ E_{\omega_j 0}\sin^2[\pi(t-T/2\tau], & T+\tau<t<T+2\tau;\\ 0, & otherwise,\end{cases} \tag{2.4}$$

with $\omega_j=\omega,2\omega$ for the fundamental and second harmonic fields respectively. Thus the carrier frequencies are equal to ω and 2ω respectively, τ is the rise and fall time of the pulse, and T is the duration of the constant amplitude portion of the pulse. $\vec{E}_{\omega 0}$ and $E_{2\omega 0}$ are the maximum amplitudes of the two fields. Numerical methods are used to solve the Schrödinger equation up to time $t=T+2\tau$, starting with the ground state $|\psi(x,0)>$ as the initial condition. At later times $(t>T+2\tau)$ the external field is equal to zero, so the resulting wave function can be analyzed in terms of free solutions of the Schrödinger equation. Thus the probability amplitude for the system to remain in the ground state can be found by projecting the final wave function $|\psi(x,T+2\tau)>$ onto the ground state wave function. Similarly, the instantaneous ionization probability can be defined as

$$P_{ion}(t)=1-|<\psi(x,0)|\Psi(x,t)>|^2. \tag{2.5}$$

This is physically meaningful only for $t>T+2\tau$, since we cannot turn the pulse off instantaneously. Nevertheless, this is still a useful quantity with which to analyze the ionization process, especially in the perturbative regime. The spatial distribution of the ionized part can be described by projecting out the bound state part:

$$|\Psi_{ion}(x,t)>=|\Psi(x,t)>-|\psi(x,0)><\psi(x,0)|\Psi(x,t)>. \tag{2.6}$$

Since the potential is short-ranged, we may define ionization probabilities in the "+" and "-"directions by

$$\begin{cases}\rho_+(t)=\int_0^\infty dx<\Psi_{ion}(x,t)|\Psi_{ion}(x,t)>,\\ \rho_-(t)=\int_0^\infty dx<\Psi_{ion}(x,t)|\Psi_{ion}(x,t)>,\end{cases} \tag{2.7}$$

which represent the ionization probabilities for the photoelectron to be ejected into "+" and "-" directions respectively. It is this difference in ionization probability that gives rise to a space charge field leading to second-harmonic generation in the fiber. We are in the processes of numerically solving the above Schrödinger equation (2.2) for a wide range of parameters, for laser intensities from perturbative to nonperturbative regimes, and for various shapes and durations of the pulses. We find that strong interference effects, as utilized by AMS-91, universally characterize the ionization process, and basically confirm the physics involved in the AMS-91 model.

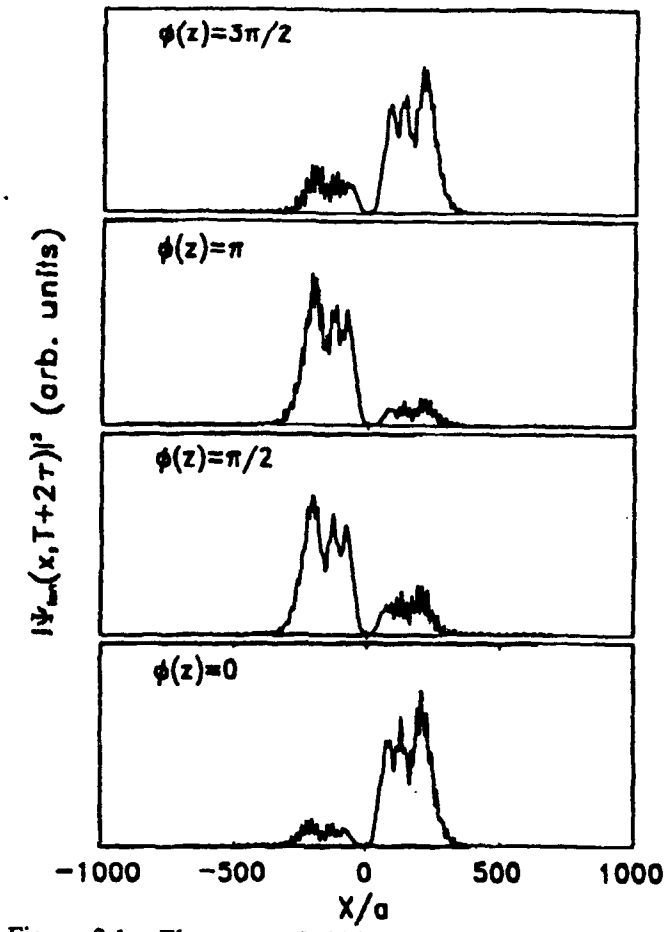

Figure 2.1. Electron probability distribution of a model potential after exposure to a field and its second-harmonic. The model potential sits at the center of the abscissa. The electron is seen to be preferentially emitted to the left or to the right depending on the relative phase of the two optical fields.

As an example of simulation results, Fig. 2.1 shows the electron probability distribution sometime after the laser field has been turned off. The model potential sits at the middle of the abscissa, $x/a = 0$. Each plot is for a different relative phase between the fundamental and second-harmonic field. Looking at the area underneath the curves we see that the electron is more likely to go to the left or to the right depending upon the relative phase of the fields. Somewhere in-between the phases shown, the electron probability will be equal for left and right propagating electrons. Figure 2.2 shows the modulation index, given by $(\rho_+ - \rho_-)/(\rho_+ + \rho_-)$, as a function of the relative phase for specific field intensities.

We note in Fig. 2.2 that the maximum modulation index occurs neither at π or $\pi/2$, thus in general there will be both gain and a phase shift caused by the $\chi^{(2)}$ grating. These calculations are still under way in order to determine, for example, how the phase of

maximum modulation index changes as a function of the absolute intensities of the optical fields.

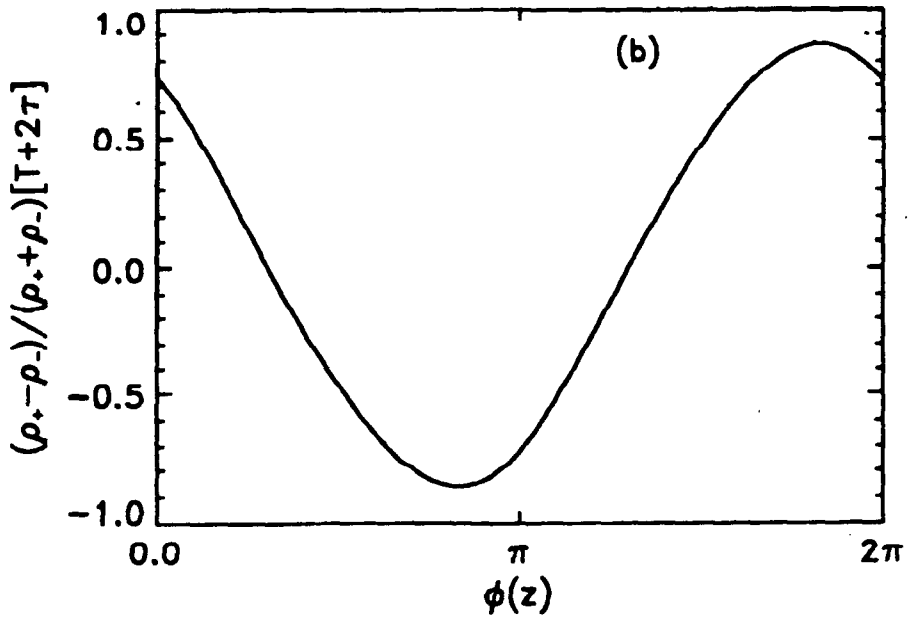

Figure 2.2. Modulation index versus relative phase between the fundamental and the second-harmonic. To the extent that the modulation index is non zero at a phase of $\pi/2$, there is gain for the self-organized growth of the second-harmonic light.

3. SELF-ORGANIZING PHOTOREFRACTIVE DEMULTIPLEXER

We are very excited about our progress in understanding the dynamics of photorefractive oscillators. The motivation for understanding the dynamics is to subsequently control, and then synthesize a given, desired, behavior from a photorefractive circuit. Based upon some new understanding we demonstrated a photorefractive circuit that self-organizes to demultiplex signals from a multimode fiber. This circuit is described in more detail below. As a spin-off of this work (funded under separate contract with NSF and AFOSR) we are working on an integrated optics version of the self-organizing demultiplexer.

We wish to point out that it is not the demultiplexer *per se* that maintains our interest, rather, the demultiplexer is the prototype for a wide variety of self-organizing circuits. By understanding and optimizing demultiplexer performance, so do we pave the way for a greater number of self-organizing processors.

We have demonstrated a self-organizing photorefractive circuit which demultiplexes a beam having two signals imposed on separate optical carrier frequencies into two beams, each containing one of the signals on its carrier.[3] Unlike conventional demultiplexing techniques we require little a priori knowledge about the carrier frequencies. The signal channels must be spatially uncorrelated and their frequency separation must be more than the photorefractive response bandwidth (Hz-KHz). The optical circuit uses no local oscillator, and the photorefractive response bandwidth places no upper bound on the

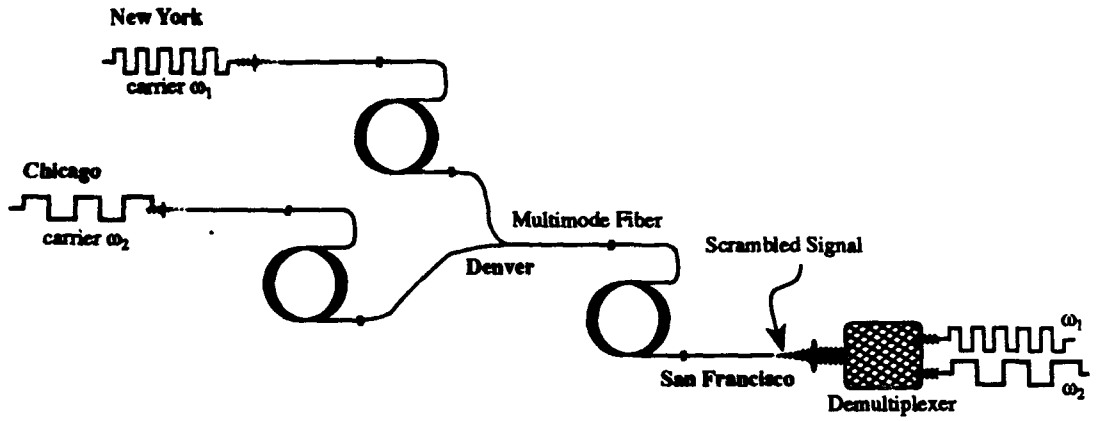

Figure 3.1 A conceptual application for a demultiplexer. Two telephone conversations, symbolized by a high and a low frequency square wave, modulate their respective optical carriers ω_1 and ω_2. These two signals are carried by multimode fibers, then both are carried by a single multimode fiber. At the output, the signals will be spatially scrambled. The demultiplexer's task is to separate the two channels.

channel bandwidth. Experimental results for demultiplexing a beam having two signals, with a BaTiO3 circuit, show contrast ratios of better than 40:1 at the outputs.

Here we review the characteristics of the demultiplexer in the context of a model application in which two signals sources share a common multimode fiber. Consider the task of demultiplexing a number of signals carried on a multimode fiber, and assume we have no a priori information about the carrier frequencies other than they are different. How can the channels at the output of the fiber be separated? One might use a grating, but then the carriers would need to be very well separated in wavelength, by at least an angstrom or so, and we do not know ahead of time that they are. One might use interferometric techniques, but these require additional frequency scan and locking electronics that must also avoid possible degeneracies in resonance conditions. To make things worse, neither approach can handle the high spatial content of the speckle patterns in a straightforward manner. We suppose that the signals are telephone conversations modulating separate laser diodes, say, residing in two cities, New York and Chicago (see Fig. 3.1). The signals are combined in one multimode fiber in Denver and in San Francisco, they are completely spatially mixed. The task is to separate the signals. The output of the multimode fiber is a very complicated speckle pattern. A self-organizing circuit can separate the channels simply by recognizing that the two signals are independent in both space and time.

Figure 3.5 shows an experimental schematic demonstrating a self-organizing photorefractive demultiplexer. Two carrier frequencies are generated from a single laser using acoustooptic modulators; one upshifting the laser frequency by 140 MHz, the other downshifting by the same amount. Square wave signals are imposed upon their respective carriers by modulating the acoustooptic cells. Both signals are injected into a multimode fiber. The output from this fiber is a spatially scrambled (speckle pattern) combination of the two signals.

The speckle output from the fiber pumps a dual ring photorefractive oscillator circuit. One detector looks at the output from each of these rings, as shown in Fig. 3.5. Because of the mode competition between the rings, the resulting dynamics gives rise to demultiplexing behavior of the circuit. Figure 3.6 shows the time evolution of the oscillating intensity in the two rings. Each of the two oscilloscope traces indicates the extent to which each signal is present in each ring as a function of time. At steady-state, each ring oscillates with only one signal carrier; each ring having taken a different carrier. Fig. 3.7 shows the steady state output seen by each of the two detectors shown in Fig. 3.5. Here again, we see the two rings have chosen different signals. There is a small amount of crosstalk in the signals, approximately 40:1.

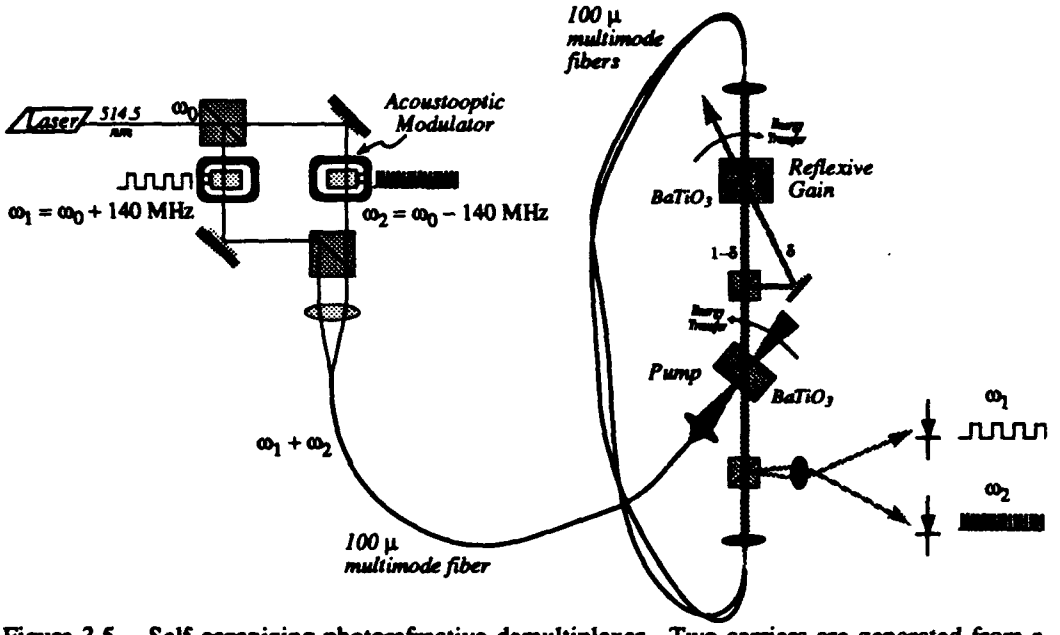

Figure 3.5. Self-organizing photorefractive demultiplexer. Two carriers are generated from a single laser by a pair of acoustooptic modulators. Square wave signals are imposed on the modulators. Both signals are injected into a multimode fiber. The speckle pattern that appears at the output of the multimode fiber pumps a photorefractive dual ring oscillator. The system self-organizes in such a way that in steady state, one of the signals oscillates in one ring, the other signal oscillates in the other ring. Though it may be slow to organize, once it does so the system demultiplexes as any passive device would. The signal bandwidth is limited only by the round-trip travel time of light around the rings to roughly 1GHz

While the demultiplexer circuit was working during the latter part of the previous year, we have made a number of improvements in the design and the stability which have yielded better performance. This work is described in some detail in Ref. [3]. We also attempted a number of demultiplexer designs employing mutually pumped phase conjugators. In principle, these have some advantages in simplicity but in practice we were never able to make them work as well as the ring resonator design. For the ring resonator we obtained signal separations of up to about 40:1, while for the phase-conjugator designs we obtained about 5:1 at best.

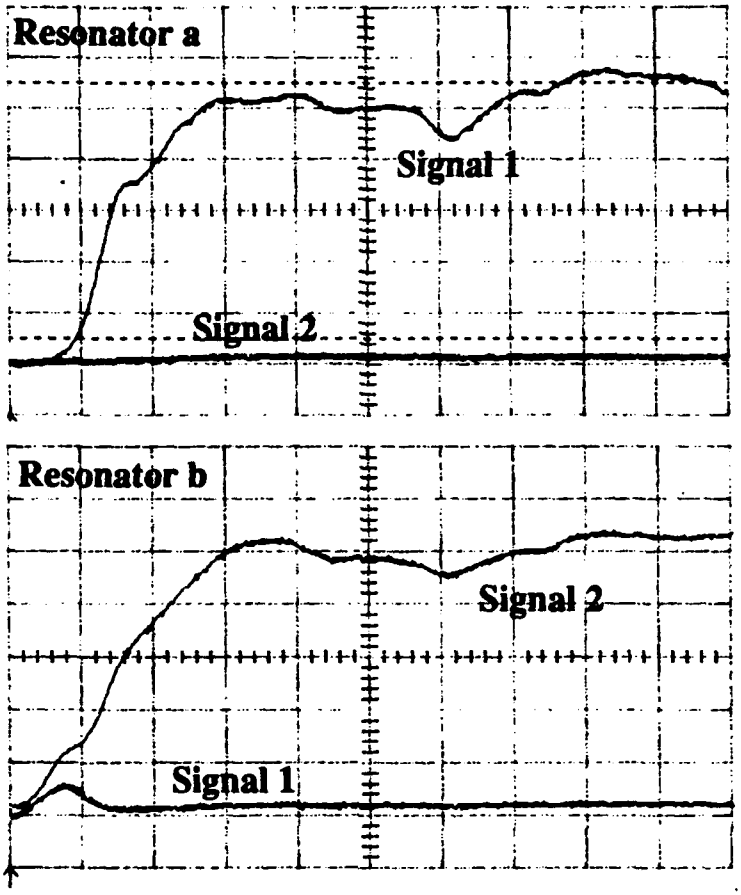

Figure 3.6. Mode evolution of demultiplexer shows the self-organizing behavior. The upper oscilloscope trace shows the intensity oscillating in one resonator (a) at each signal frequency. The lower trace shows the intensity oscillating in resonator b. Note that after some time resonator a oscillates entirely in signal 1 while resonator b oscillates entirely in signal 2. (The labeling of the resonators and signals is arbitrary.)

The progress in understanding the dynamics in ring circuits has been aided by numerical simulation of our photorefractive circuits. We have made numerous numerical studies on both classes of demultiplexers to investigate issues of stability and time response. Of particular interest is the mechanism by which symmetry between the two ring - signal combinations — after all, the circuit is nominally symmetrical between the two cases: ring a oscillating in signal 1 and ring b oscillating in signal 2. For the time being we do not know whether the final state is dictated by biases that make the rings somewhat different, or from noise, which, computer simulations show, can cause spontaneous breaking of the symmetry.

Current investigations in self-organizing circuits

Ongoing work looks at continuous resonator circuits. Whereas the demultiplexer and related circuits have a discrete number of rings, it is interesting to study dynamics of oscillators having a continuum of ring paths. In principle this is possible with appropriate

design of an open resonator. Obtaining the proper competitive dynamics is the key, and this is now being looked at by computer simulation. Why is a continuum circuit design interesting? Our motivation comes from a class of neural network models called topology preserving maps. In these systems the networks have a notion of topology built into them: any given unit is connected to a neighborhood of other units. The self-organizing behavior of these networks is fascinating: they can discover the spatial topology of the input space. They have been shown to be useful in pattern recognition and speech processing, for example.

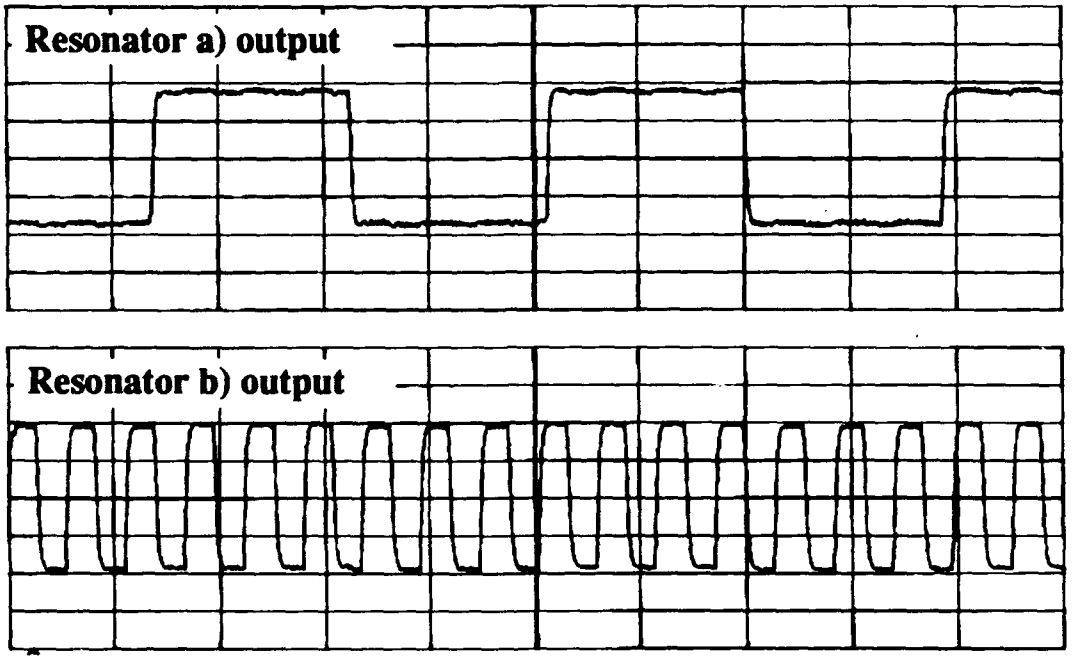

Figure 3.7. Steady state output intensity of self-organizing demultiplexer. The two resonators have divided between them the two spatially scrambled signals of the pump. A small amount of crosstalk exists: One signal contaminates the other by about 1:40.

REFERENCES

[1]U. Österberg and W. Margulis, Opt. Lett. **11**, 516 (1986).
[2] D. Z. Anderson, V. Mizrahi, and J. E. Sipe, Opt. Lett. **16**, 796 (1991).
[3]M. Saffman and D.Z. Anderson, Opt. Lett., **16**, 300 (1991).